Scientia Iranica, Vol. 15, No. 5, pp 541–553

SCIENTIA
IRANICA

A Numerical Study of Chamber Size and Boundary Effects on CPT Tip Resistance in NC Sand

M.M. Ahmadi[1,*] and P.K. Robertson[2]

A numerical modeling procedure was used to quantify calibration chamber size and boundary effects for cone penetration testing in sand. In the numerical analyses, chamber diameter and boundary conditions were varied to investigate the effects of chamber size and boundary conditions on cone tip resistance. These analyses show that, for loose sand, a chamber-to-cone diameter ratio of 33 is sufficient for the boundaries to have no influence on the cone tip measurements. However, for very dense sand, the numerical analyses show that the chamber-to-cone diameter ratio should be more than 100 to ensure that boundaries have no influence on cone tip measurements. Numerical analysis indicates that, not only the sand relative density but its stress state is also a significant factor in influencing the chamber size effects. The results of the numerical analyses were compared to existing empirically based relationships. Suggestions are provided to reduce the effects of chamber size and boundaries on cone tip resistance measurements in sand.

INTRODUCTION

The purpose of calibration chamber testing is generally to study the response of the Cone Penetration Test (CPT), under well defined and well controlled conditions, to the relative density, stress state and stress history of sand. The results of these tests can provide empirical relationships between cone penetration resistance (q_c), sand relative density (Dr) and stress state. Holden [1] presented a historical perspective of calibration chamber testing. Bellotti et al. [2,3], and Salgado et al. [4], among others, discussed calibration chamber test procedures in detail. Ghionna and Jamiolkowski [5] and Been et al. [6] presented a critical overview of the shortcomings of calibration chamber testing, especially with regard to chamber boundary conditions.

Ideally, calibration chambers should be of sufficient size that the CPT results are not affected by the calibration chamber size and boundaries. However, calibration chambers have finite dimensions with defined stress and/or strain conditions at the chamber boundaries, and the boundary conditions imposed on the chamber may not represent the real field situation. In order to simulate the semi-infinite soil mass in the field, the calibration chamber boundary conditions often represent two extreme limits of either constant stress or zero displacement on the horizontal and vertical boundaries. These boundary conditions can influence the cone tip resistance measured in calibration chambers if the chamber is not of sufficient size.

Depending on whether stresses are kept constant or displacements are zero at the lateral and bottom sample boundaries, there are four different types of boundary condition that can be applied during the experimental testing of penetration in the calibration chamber [5]. These four types of boundary condition are listed in Table 1; and are given the symbols BC1 to BC4. For BC1 types of boundary condition, constant stresses are maintained at the bottom boundary, as well as at lateral directions, in the calibration chamber. These stresses are equal to the stresses after the completion of K_0 consolidation. For BC3 types of boundary condition, a constant stress is imposed at the bottom boundary during penetration testing, while the displacement of the lateral boundary is kept at zero.

1. *Department of Civil Engineering, Sharif University of Technology, P.O. Box 11155-9313, Tehran, Iran.*
2. *Department of Civil and Environmental Engineering, University of Alberta, Edmonton, Alberta, Canada, T6G 2G7.*
*. *To whom correspondence should be addressed. E-mail: mmahmadi@sharif.edu*

Table 1. Boundary conditions available in calibration chamber tests.

Type of Boundary Condition	Lateral Boundary Condition	Bottom Boundary Condition
BC1	Horizontal stress = constant	Vertical stress = constant
BC2	Horizontal strain = 0	Vertical strain = 0
BC3	Horizontal strain = 0	Vertical stress = constant
BC4	Horizontal stress = constant	Vertical strain = 0

Note: For horizontal and vertical boundaries with zero strain, the corresponding boundary nodes are fixed in the horizontal and vertical directions, respectively. Similarly, for horizontal and vertical boundaries with constant stress, the corresponding boundary nodes are under a constant horizontal and vertical stress, respectively.

Calibration chamber testing with BC1 and BC3 type boundary conditions are frequently performed in CPT experimental research. For BC2 types of boundary condition (BC2), displacement at all the boundaries (radial and bottom) is kept at zero during testing and, for BC4 types of boundary condition, a constant stress is applied at the radial boundary, while the bottom boundary is restrained, i.e., the vertical displacement at the bottom boundary is kept at zero during the testing procedure.

These four different boundary conditions do not simulate field conditions perfectly. The larger the chamber size (relative to the size of the cone), the less significant is the difference between the CPT results obtained in the chamber and the results obtained in the field.

The effects of chamber size and boundary conditions on the CPT tip resistance values measured in a calibration chamber have been recognized for many years. Parkin and Lunne [7], based on CPT results for two different chamber and penetrometer sizes, concluded that, for loose sands, chamber size and boundary conditions generally do not have a significant effect on cone tip resistance. However, for dense sands, they concluded that the effects could be considerable. Lunne and Christophersen [8], based on chamber test results on Hokksund sand, suggested that, for a chamber-to-cone diameter ratio of 50, the difference between tip resistance obtained in the chamber and in the field should be small. To minimize chamber size and boundary effects, Hsu and Huang [9] developed a new experimental system capable of simulating an axisymmetric field condition. They argue that the system is capable of duplicating field conditions where the lateral boundary extends to infinity and, therefore, enabling cone penetration tests to be calibrated under minimal boundary effects.

Jamiolkowski et al. [10] proposed an empirical formula to relate CPT tip resistance obtained in the chamber to tip resistance in the field. For conventional calibration chamber sizes and standard cone sizes, they suggested the following simplified relationship:

$$q_{c,\text{field}} = q_{c,cc}\left(1 + \frac{0.2(Dr\% - 30)}{60}\right). \quad (1)$$

In the above formula, $q_{c,cc}$ is the experimental value of tip resistance observed in the calibration chamber, Dr is the relative density and $q_{c,\text{field}}$ is the corrected tip resistance expected to be measured in the field for the same sand with the same relative density and in-situ stresses as in the chamber. The above formula implies that, for loose sand with a relative density of 30%, the experimental results in the chamber and the field are basically similar and no calibration chamber size effect should be considered. However, as the relative density of sand in the chamber increases, the size effect will become larger. The above formula is valid for a standard cone penetrometer with a projected cone area of 10 cm^2 in a conventional 1.2 m diameter chamber and was based on the experimental results obtained in calibration chamber tests under BC1 type boundary conditions (see Table 1).

Schnaid and Houlsby [11] have documented, experimentally, the importance of chamber size effects on the ultimate cavity stress obtained from pressuremeter tests. They suggested that finite chamber dimensions affect cone tip resistance to, approximately, the same extent as the pressuremeter.

Mayne and Kulhawy [12] developed the following empirical equation to relate tip resistance measured in the chamber to tip resistance in the field:

$$q_{c,\text{field}} = q_{c,cc}\left[\frac{(D_{cc}/d_{cone}) - 1}{70}\right]^{-Dr(\%)/200}, \quad (2)$$

where D_{cc} is the diameter of the calibration chamber and d_{cone} is the diameter of the cone.

As noted in Equation 2, Mayne and Kulhawy [12] assumed that, regardless of the relative density and

stress state, a chamber-to-cone diameter ratio of about 70 is sufficient to achieve the "free field" condition.

Salgado et al. [13] proposed a penetration resistance theory to quantify chamber size effects and concluded that sand relative density, stress state and intrinsic soil parameters are the most important factors to be considered in the magnitude of the chamber size effect. The procedure suggested by Salgado et al. [13] is valid only for BC1 and BC4 type boundary conditions.

Wesley [14] argued that, in a conventional calibration chamber test, the vertical stress in front of the cone tip is limited by the applied pressure at the base, and the vertical stress above the cone is reduced. He argued that this is in contrast to a field situation, where the vertical stress above the cone remains essentially constant (equal to the overburden pressure), while the vertical stress below the cone increases, depending on the cone force and the properties of the soil. This assumed reduction of vertical stress in front of the cone can give rise to a reduction of cone tip resistance in the chamber and, hence, Wesley [14] provided a method for correcting the results of cone tip resistance measurements in chamber tests, where a constant vertical stress is applied at the chamber bottom boundary.

While these experimental observations have been known for some time, numerical procedures to correctly model the CPT penetration process in sand, in a calibration chamber with all the boundary conditions, are inadequately addressed in the literature.

In this paper, the effects of chamber size and boundary conditions will be presented, based on the numerical modeling procedure for sand suggested by Ahmadi [15], Ahmadi et al. [16] and Ahmadi and Robertson [17], to analyze the cone penetration process. Analyses were carried out for normally consolidated (K_0 equal to 0.5) dense, medium dense and loose sand. Numerical predictions of tip resistance in the calibration chamber, as a function of chamber size and boundary condition, are compared with other experimental and numerical procedures available in the literature. All analyses were performed for standard cone penetrometers, having a conical tip with a base area of 10 cm^2 and 60 degree tip apex angle. The finite difference based computer program, FLAC, [18] was used for the analyses.

CONSTITUTIVE LAW FOR SAND

In this section, a brief explanation of the constitutive law for sand is given. A detailed explanation can be found in [16].

A Mohr-Coulomb elastic-plastic model was chosen for the analysis of cone penetration. This is a simple model that can reasonably approximate the behaviour of sand. Two elastic and two plastic parameters are needed for the model. The elastic parameters are shear and bulk modulus, and the plastic parameters are friction and dilation angle.

During cone penetration, the magnitude of stresses around the cone tip becomes much larger than those far from the cone tip [19]. Since the response of sand is stress dependent, model parameters should be different in the near and far fields. Hence, in simulating the penetration process, the Mohr-Coulomb soil parameters are considered to be stress dependent.

The stress dependent relation for the shear (G) and bulk (K) modulus can be written as:

$$G = K_G P_A \left(\frac{\sigma'_m}{P_A}\right)^n, \tag{3}$$

$$K = K_B P_A \left(\frac{\sigma'_m}{P_A}\right)^n, \tag{4}$$

where σ'_m is the mean effective stress and P_A is the atmospheric pressure, or a reference pressure equal to 98.1 kPa. The exponent, n, can range from 0.2 to 0.7 and is taken to be 0.6 in this study. This chosen value of n has produced numerical predictions of cone tip resistance that are in better agreement with experimental measurements. This is discussed in detail in Ahmadi et al. [16]. K_G and K_B are the shear and bulk modulus numbers, respectively, with values shown in Table 2. These values depend only on sand relative density and are in the range reported by Byrne et al. [20]. The ratio of K_G/K_B is relatively independent of Dr and shear stress and is approximately equal to 0.6. This means that Poisson ratio is assumed to be 0.25 in this analyses, which is a reasonable value for sand. These analyses show that the Poisson ratio does affect the predicted values of tip resistance, but its influence is small. This is discussed in Ahmadi et al. [16].

The Mohr-Coulomb model used also needs to be defined in terms of the plastic parameters, i.e., friction angle and dilation angle. Baligh [19] argues that, since the tip resistance obtained in granular material often exceeds the level of stresses ordinarily encountered in other applications, a realistic analysis of tip resistance in sand must, therefore, be based on the response of

Table 2. Parameters used for deformation and shear strength of Ticino sand.

Dr%	K_G	K_B	ϕ'_0 (deg)	α (deg)
45	195	325	38.2	4.2
65	230	385	40.2	6.5
85	290	480	42.9	8.1

Dr: Average relative density of the tested specimens at the end of consolidation.

ϕ'_0: From triaxial compression test.

the soil at elevated stresses. This response differs from common behaviour in two important aspects:

a. The induced high stresses result in a decrease of the angle of internal friction, i.e. the Mohr-Coulomb failure envelope is not straight but is non-linear;

b. The induced high stresses cause a significant decrease in volumetric strain in the sand during penetration, even for dense granular media [19].

The shear strength parameters of Ticino sand were determined, based on a series of triaxial tests carried out by ENEL/ISMES [21] and the curvilinear formula proposed by Baligh [19]:

$$\tau_{ff} = \sigma'_{ff}\left[\tan\phi'_0 + \tan\alpha\left(\frac{1}{2.3} - \log_{10}\frac{\sigma'_{ff}}{P_A}\right)\right], \quad (5)$$

where τ_{ff} is the shear stress on the failure surface at failure, σ'_{ff} is the effective normal stress on the failure surface at failure, α is the angle that describes the curvature of the failure envelope and ϕ'_0 is the secant angle of friction at σ'_{ff} equal to 2.72 P_A. Table 2 shows the published values of ϕ'_0 and α obtained from specimens of Ticino sand at three different relative densities [21]. As suggested by Baldi et al. [21], the friction angle values used for analyses are based on triaxial compression tests. Values in Table 2 indicate that, with higher relative densities, the friction angle values become larger. It can be seen in Equation 5 that, at higher stress levels, i.e. at higher values of σ'_{ff}, the friction angle decreases.

The dilation angle at failure was computed from the friction angle at failure and the constant volume friction angle as follows:

$$\sin\psi = \sin\phi'_f - \sin\phi_{cv}, \quad (6)$$

where:

ψ = dilation angle,
ϕ'_f = effective friction angle at failure,
ϕ_{cv} = constant volume friction angle for Ticino sand, measured to be 34.8 degrees, as described by Lo Presti et al. [22].

NUMERICAL MODEL OF CONE PENETRATION

In this section, a brief explanation of the numerical procedure used to model the penetration mechanism is given. Full details of the numerical approach are beyond the scope of this paper and are discussed in detail by Ahmadi et al. [16].

In order to simulate the penetration mechanism, the soil nodal points located along the cone path are pushed away in a systematic process, which starts from the top of the grid and can continue to any desired depth into the grid. This process simulates penetration in the field, as the cone penetrates downward in the ground pushing the soil particles to the side, horizontally as well as vertically.

Figure 1 shows a close-up view of the inner boundary nodal points at an arbitrary depth inside the grid. All these inner boundary points are displaced, horizontally as well as vertically. Figure 1 shows that, during the modeling procedure, the nodal point, A, has already been pushed away from its initial location, A', by giving a horizontal as well as vertical downward displacement. The line, A'A, in the figure shows the displacement vector for this point. The nodal points, B, C and D, are now being pushed away from the inner boundary. The nodal point, B, has just been displaced sufficiently and will no longer be pushed. As the process of imposing displacement on point B is halted, point E starts to be displaced and this process continues systematically to any desired depth.

In the numerical analysis, the nodal points associated with the cone face, i.e. points B, C, D and E in Figure 1, are given a displacement vector that has two components: One in the horizontal direction and the other in the vertical direction downward. While the magnitude of the imposed horizontal component of the displacement is clear, there are no such obvious compatibility restraints for the vertical displacements around the cone. The effect of the vertical component of applied inner boundary displacement was first examined by considering the ratios of vertical to horizontal in the ranges of zero to 1.

The analysis showed that the larger the verti-

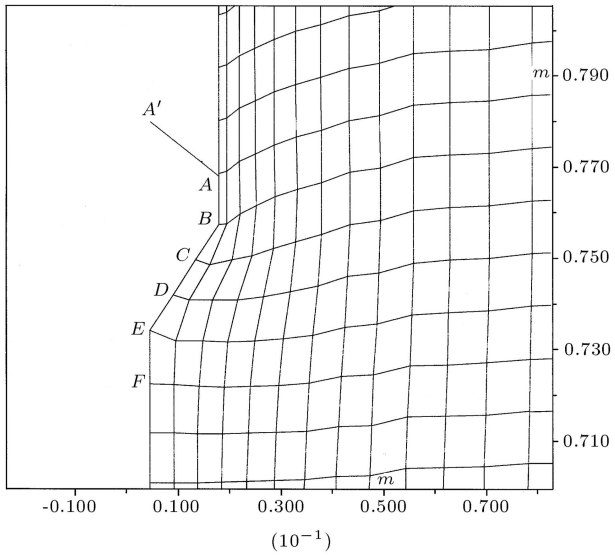

Figure 1. A close-up view of the inner boundary nodal points of the numerical grid at an arbitrary depth of penetration. The height and the radius of the grid are expressed in meters.

cal displacement component, the larger the predicted values of tip resistance. For cases when the vertical component of the imposed displacement vector is zero, i.e. no downward vertical displacement is imposed, the numerical analysis indicates that the predicted values of the tip resistance are much less than those measured experimentally, and the deformation pattern around the cone does not show a vertical downward displacement, similar to that observed in experiments. For cases in which the downward vertical component of the imposed displacement is large (e.g. equal to the horizontal component), the numerical analysis predicts values of tip resistance that are larger than those measured experimentally. It was concluded that a reasonable value for the vertical component of the imposed displacement should lie in the range between these two extremes.

A large number of numerical analysis was performed, in which the vertical displacement was varied in this range. It was found that a vertical downward displacement, equal to 60% of the horizontal component of displacement imposed on the inner boundary, would produce tip resistance predictions that agree best with experimental measurements. It was also observed that the displacement pattern obtained in the numerical analysis was similar to the experimental observations of van den Berg [23].

This modeling procedure imitates the penetration process in a realistic way. The penetration modeling starts at the top of the grid, progresses into the grid and can end at any desired depth in the grid; meaning that the modeling process is simulating the cone moving downward in the ground penetrating different soil layers with different properties. An evaluation of the modeling approach, comparing both field and calibration chamber experimental results, is provided by Ahmadi et al. [16]. Figure 2 shows the full grid with the location of the cone tip at an arbitrary depth in the grid. The numerical grid chosen for this study has a height of 1.5 m, similar to the height of most calibration chamber tests used currently around the world, and a diameter ranging from 1.2 m to 4.0 m. This range in diameter was chosen to study the effects of calibration chamber size on cone tip resistance values. This corresponds to a chamber-to-cone diameter ranging from about 33 to 112, for a standard 10 cm^2 cone (i.e. cone diameter of 35.7 mm). The total height of the grid does not play a significant role in the analyses, since the predicted values of tip resistance at mid-height were used. Figure 2 shows a typical axisymmetric grid used in the analysis. For this figure, the diameter of the grid is 1.2 meters.

Because the problem has symmetry about the vertical axis, the axisymmetric option was used for this three dimensional problem, in order to reduce the number of elements in the solution procedure. To

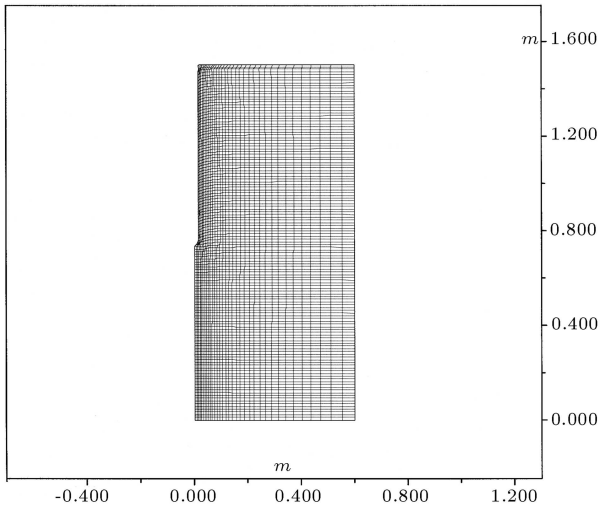

Figure 2. An axisymmetric grid showing cone tip at an arbitrary location at the centreline of the grid. The height and the radius of the grid are expressed in meters.

comply with the large deformations occurring in the vicinity of the cone tip, the large strain modeling procedure implemented in the code was used.

To study the boundary condition effects on cone tip resistance, the numerical grid was placed under different types of boundary condition to simulate the boundary conditions applied during calibration chamber testing, which are presented in Table 1.

ANALYSIS RESULTS

Figure 3 shows the result of the analyses of cone penetration in dense sand for all four different boundary conditions. The sand relative density in this series of

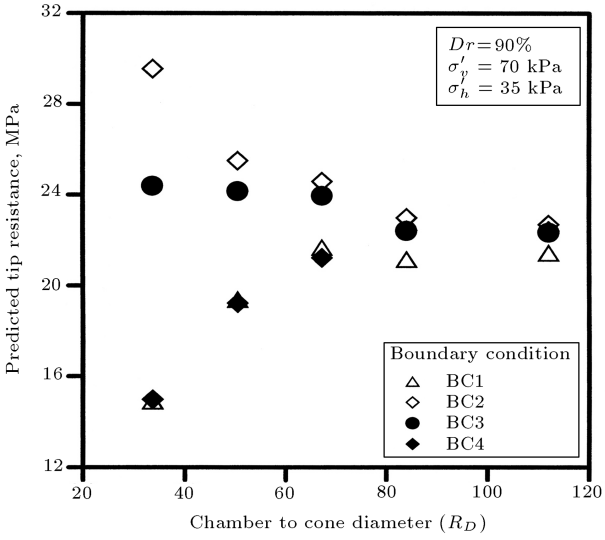

Figure 3. Effect of chamber size and boundary condition on tip resistance (predictions for dense sand); $Dr = 90\%$, $\sigma'_v = 70$ kPa and $K_0 = 0.5$.

analysis was 90%, with an effective vertical stress of 70 kPa and $K_0 = 0.5$, giving a horizontal effective stress of 35 kPa. The high value of sand relative density, together with low values of the stress state selected as input for these analyses, characterizes very dense sand with a high degree of dilation. As stated earlier, analyses were carried out for chambers of different diameter, namely 1.2 m, 1.8 m, 2.4 m, 3.0 m and 4 m.

The ordinate in Figure 3 represents the predicted cone tip resistance (in MPa) obtained for each analysis carried out under different boundary conditions and chamber diameters. The analysis predicts the tip resistance continuously for the full height of the chamber (grid), and the tip resistance values taken in this paper are the values that are predicted at the mid-height of the numerical grid [16]. This conforms to the experimental values in the database, where the mid-height tip resistance values were reported [24].

As can be seen in Figure 3, the cone tip resistance is a function of boundary condition and the ratio of chamber-to-cone diameter. For BC1 boundary conditions, the tip resistance increases as the ratio of chamber-to-cone diameter increases. Figure 3 also shows the same trend for BC4 boundary conditions. The numerical values of tip resistance obtained for both BC1 and BC4 boundary conditions, for most values of chamber-to-cone diameter ratio, are very close.

For BC2 boundary conditions, the numerical analyses show that the predicted tip resistance decreases as the chamber-to-cone diameter ratio increases. For BC3 boundary conditions, the predicted tip resistance is almost constant with a predicted value of 24.3 MPa in a 1.2 m diameter chamber and a value of 22.3 MPa in a 4.0 m diameter chamber.

Figure 3 shows that, for values of a chamber-to-cone diameter of 33, there is a large difference in cone tip resistance for different boundary conditions for very dense sand at low stresses. This difference is especially large between BC2 boundary conditions and both BC1 and BC4 boundary conditions. This indicates that, for very dense sand at very low confining stresses, the results of cone tip resistance obtained in most commonly used calibration chamber tests are significantly affected by the boundary conditions. In this case, a chamber-to-cone diameter ratio of about 100 or more is needed to measure tip resistance during chamber testing that is not affected by the chamber boundaries.

Figures 4 and 5 show the results of numerical analyses of cone penetration for all four boundary conditions and different ratios of chamber-to-cone diameter, for medium dense ($Dr = 70\%$) and relatively loose ($Dr = 50\%$) normally consolidated sands, respectively. Medium dense sand was characterized by a relative density of 70%, with an effective vertical stress of 300 kPa and effective horizontal stress of 150 kPa (i.e. K_0 of 0.5). The loose sand was characterized by a low value of relative density ($Dr = 50\%$) and high values of stress state. In the analysis presented in Figure 5 for loose sand, the effective vertical stress was taken to be 700 kPa and the effective horizontal stress to be 350 kPa. Figure 4 shows that, for a given chamber-to-cone diameter (R_D) value, the difference in predicted tip resistance values for boundary conditions BC1 (or BC4) and BC2 obtained in the analyses for medium dense sand, is appreciably less than that obtained for the very dense sand (Figure 3). For loose sand, this difference is even smaller. This is seen in Figure 5

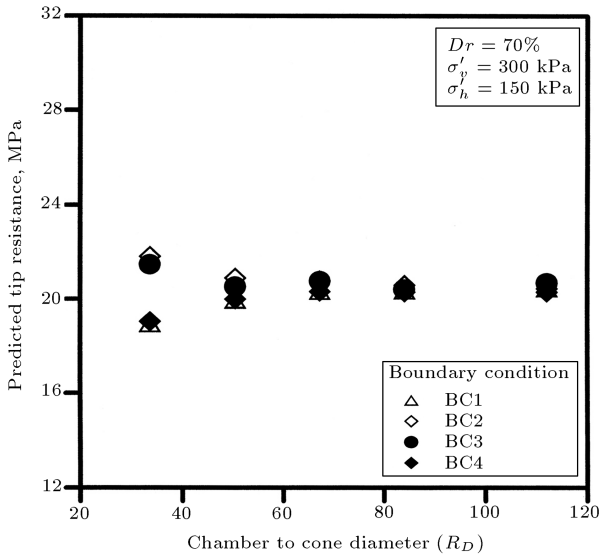

Figure 4. Effect of chamber size and boundary condition on tip resistance (predictions for medium dense sand); $Dr = 70\%$, $\sigma'_v = 300$ kPa and $K_0 = 0.5$.

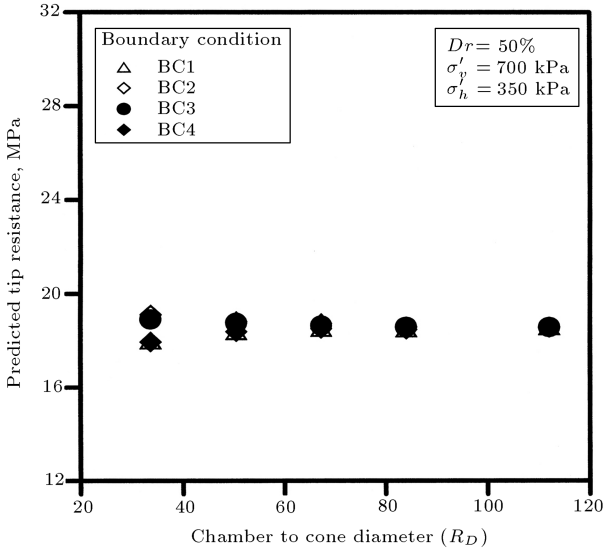

Figure 5. Effect of chamber size and boundary condition on tip resistance (predictions for loose sand); $Dr = 50\%$, $\sigma'_v = 700$ kPa and $K_0 = 0.5$.

where, for any value of chamber-to-cone diameter ratio of more than 33.6 and for any type of boundary condition, the predicted tip resistances do not differ appreciably and are about 18.6 MPa. These results imply that the zone of influence around a penetrating cone in sand is small if the sand is very loose, but large when the sand is very dense.

The analyses presented in this study for normally consolidated sand with constant lateral stress (i.e. BC1 or BC4 boundary conditions) and for a given sand relative density and stress state in conventional chamber sizes (1.2 m diameter) using a standard 10 cm^2 cone, indicate that the predicted values of cone tip resistance are generally underestimated compared to those in the field. In contrast, the analyses show that, for boundary conditions with zero lateral strain (i.e. BC3 or BC2) simulating rigid circumferential boundaries, q_c values in the chamber are generally higher than those measured in the field. This is because, for a constant lateral stress condition, the magnitude of horizontal stresses at the boundary remains constant, whereas, for cone penetration in the field, the value of horizontal stress at a radius similar to the chamber radius increases as the cone penetrates into the ground pushing the soil particles to the side and mobilizing higher lateral stresses. In other words, in the field, horizontal stress, especially at locations sufficiently close to the cone tip, increases during penetration and this produces field values of penetration resistance that are larger than those measured in conventional calibration chambers with a constant lateral stress boundary.

However, the situation is quite different for cone penetration with rigid lateral boundaries. In the numerical analysis for this type of boundary condition, the cone penetration induces large horizontal stresses around the cone, because of the rigid boundaries. This is because, in the case of rigid boundaries, a larger reaction from the boundaries can be mobilized and, hence, larger tip resistance values are predicted. Since, in the field, the boundaries in the proximity of the cone are not rigid, it is physically expected that the induced horizontal stresses may be smaller, compared with numerical predictions obtained in the analysis of cone penetration with rigid lateral boundaries, and therefore, smaller tip resistance values can be measured in the field. In other words, in the numerical analysis, the boundaries are assumed to be completely rigid, whereas, under real field conditions similar to other practical situations, a completely rigid boundary condition would not be possible. This is also observed by Salgado et al. [4], where it is argued that calibration chamber tests with BC3 type boundary conditions have shown some lateral flexibility, even though these boundaries are theoretically assumed to be rigid.

EVALUATION WITH EXPERIMENTAL STUDIES

There are two possible approaches to evaluate and compare numerical and experimental results. One is to compare the predicted numerical values of tip resistance with experimental values for sands under similar density and stress states. The second is to compare the trend of numerical values, due to calibration chamber size and boundary conditions, with experimental results. Ahmadi et al. [16] have already carried out a detailed comparison between predicted numerical values and measured experimental values, which have shown a good comparison.

The focus of this paper is to study the influence of calibration chamber size and boundary effects on cone tip resistance in sand. Unfortunately, few experimental research programs have been carried out to specifically address calibration chamber size and boundary effects. This is especially true for Ticino sand. Hence, comparison is made with other sand types. Even in these circumstances, all needed information from the testing program was unavailable to carry out a one-to-one comparison between measured and predicted tip resistance values. Therefore, the general response between numerical predictions and experimental observations is investigated at this stage.

Based on experimental observations, Parkin [25] presented data for measured CPT tip resistance in the calibration chamber versus the ratio of chamber-to-cone diameter (R_D) for normally consolidated Hokksund sand. These data, reproduced from [25], are shown in Figure 6. Parkin [25] did not specifically report the relative density and stress state of the sand

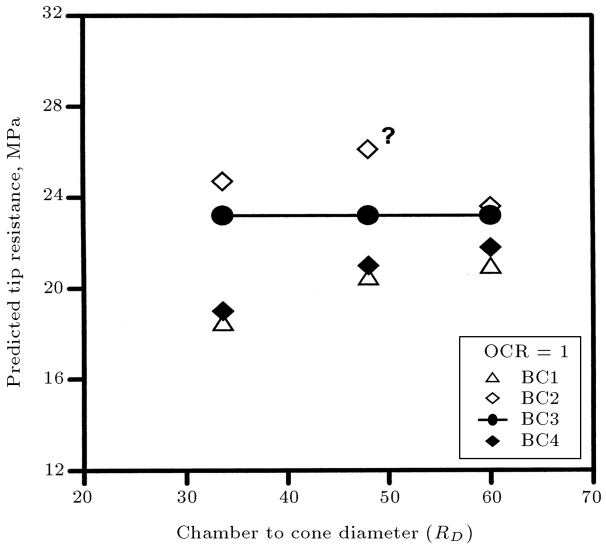

Figure 6. Effect of chamber size and boundary condition on tip resistance, based on experimental work on normally consolidated dense sand reproduced from [7].

tested in the calibration chamber and, therefore, a direct comparison could not be made.

Parkin [25] argues that, within the limits of experimental accuracy and for $R_D > 33$, there is a pronounced grouping of results. He, based on his experimental observations, notes that, for normally consolidated dense sand (Figure 6), the BC1 and BC4 results group together and are, effectively, identical. Also, the measured tip resistance for both these boundary conditions increases with an increase of the ratio of chamber-to-cone diameter (R_D). Parkin [25] also notes that, for the range of R_D values chosen in the experiments, the measured tip resistance values for BC3 type boundary conditions are essentially independent of the chamber-to-cone diameter ratio.

For BC2 type boundary conditions, the experimental measurements [25] show somewhat larger values of tip resistance for lower ratios of R_D. For higher R_D ratios, the tip resistance values converge downwards to values close to those for the other boundary conditions.

Comparing Figure 6 with Figure 3, it is seen that the numerical prediction of the response of CPT in the calibration chamber is in very good agreement with the trend of the experimental observations of Parkin [25]. Figure 3 shows that, for BC1 and BC4 boundary conditions, the tip resistance values align together for the range of R_D ratios used in the analysis, and increase as the R_D ratio increases. Figure 3 also shows a decreasing trend for BC2 results, as R_D increases.

Figure 3 shows that the predicted BC3 results are approximately constant, with slightly larger values of tip resistance for smaller values of R_D. This is close to the constant values noted in the experimental observations [25], and will be further discussed later in this paper.

Parkin [25] reports that, for loose sand, even for chamber-to-cone diameter ratios as small as 21, the chamber results are independent of boundary conditions. This is consistent with the predicted variation, shown in Figure 5, for loose sand.

For the BC2 boundary condition and for an R_D value of about 50, Parkin [25] notes that the experimental data point, shown with a question mark in Figure 6, appears to be inconsistent with other BC2 results. Parkin [25] argues that this might be a labelling error. The numerical predictions in this study confirm Parkin's observation.

COMPARISON WITH THEORETICAL STUDIES OR EMPIRICAL RELATIONS

The results of this study are also compared with the numerical results of Salgado et al. [4] and the empirical relations suggested by Jamiolkowski et al. [10] and Mayne and Kulhawy [12]. Table 3 shows this comparison for two sands with different relative densities and different stress states.

To perform a one-to-one comparison with the numerical technique of Salgado et al. [4], the same input parameters, i.e. sand relative density and stress state, used by Salgado et al. [4], were also used in the numerical analyses in this study. The numerical technique suggested by Salgado et al. [4] is only valid for BC1 (or BC4) boundary conditions; therefore, for comparison, only BC1 results are considered.

As shown in Table 3, for sand with a relative density of $Dr = 49.1\%$, vertical effective stress of 112 kPa and horizontal effective stress of 54 kPa, Salgado et al. [4] calculated the ratio, $q_{c,cc}/q_{c,\text{field}}$, to be 0.6, 0.7 and 0.8 for R_D values of 33.6, 50.4 and 67.2, respectively. Parameter $q_{c,cc}$ refers to the numerical prediction of tip resistance in the calibration chamber

Table 3. Comparison of numerical results obtained in this study with other numerical or empirical relations (for BC1 conditions).

	$Dr = 49.1\%$ $\sigma'_v = 112$ kPa, $\sigma'_h = 54$ kPa $q_{c,cc}/q_{c,\text{field}}$			$Dr = 74.9\%$ $\sigma'_v = 114$ kPa, $\sigma'_h = 48$ kPa $q_{c,cc}/q_{c,\text{field}}$		
	Calibration Chamber Diameter					
	1.2 m	1.8 m	2.4 m	1.2 m	1.8 m	2.4 m
	$R_D = 33.6$	$R_D = 50.4$	$R_D = 67.2$	$R_D = 33.6$	$R_D = 50.4$	$R_D = 67.2$
This Study	0.89	0.96	0.98	0.79	0.96	0.98
Salgado et al. [4] (Numerical)	0.6	0.7	0.8	0.52	0.65	0.75
Jamiolkowski et al. [10] (Empirical)	0.94	N/A	N/A	0.87	N/A	N/A
Mayne and Kulhawy [12] (Empirical)	0.83	0.92	0.99	0.75	0.88	0.98

R_D: Calibration chamber diameter to cone diameter

with boundaries located at a specified distance from the cone and parameter $q_{c,\text{field}}$ refers to the numerical prediction of tip resistance when boundaries are placed far enough from the cone, simulating field conditions. For the same value of sand relative density and stress state, the numerical analyses carried out in this study predict the $q_{c,cc}/q_{c,\text{field}}$ ratios to be 0.89, 0.96 and 0.98 for R_D values of 33.6, 50.4 and 67.2, respectively, as shown in Table 3. The trend of increasing the $q_{c,cc}/q_{c,\text{field}}$ ratio with an increase of R_D values is observed in both numerical techniques. However, the Salgado et al. [4] procedure predicts ratios that are significantly smaller than the values predicted in this study.

The numerical predictions in this study are also compared with those suggested by Salgado et al. [4] for dense sand. As shown in Table 3, for sand with a relative density of 74.9%, vertical effective stress of 114 kPa, and horizontal effective stress of 48 kPa, Salgado et al. [4] predicts the $q_{c,cc}/q_{c,\text{field}}$ ratios to be 0.52, 0.65 and 0.75 for R_D values of 33.6, 50.4 and 67.2, respectively. The associated values predicted in this study are 0.79, 0.96 and 0.98. As the density increases, Table 3 shows that the $q_{c,cc}/q_{c,\text{field}}$ ratio becomes smaller for both numerical techniques. This means that the boundary effects are larger as relative density increases. This is in agreement with experimental observations [25] discussed previously. Comparing the $q_{c,cc}/q_{c,\text{field}}$ ratios obtained by Salgado et al. [4] with those in this study, it is again observed that the Salgado et al. [4] procedure predicts ratios that are significantly smaller than those obtained in this study.

The numerical predictions in this study are also compared with the empirical relations suggested by other researchers. For the sand relative densities of $Dr = 49.1\%$ and 74.9% and for R_D value equal to 33.6, Jamiolkowski et al. [10], based on an empirical relation (Equation 1), suggested the values of $q_{c,cc}/q_{c,\text{field}}$ to be 0.94 and 0.87, respectively. As stated previously, the empirical relation proposed by Jamiolkowski et al. [10] is only valid for a calibration chamber of 1.2 m diameter under BC1 boundary conditions and a standard cone, resulting in an R_D value of 33.6. Their empirical relationship is not applicable for other R_D values and, hence, no values are shown in Table 3 for other R_D values.

As shown in Table 3, for sand with a relative density of $Dr = 49.1\%$, Mayne and Kulhawy [12] suggest that $q_{c,cc}/q_{c,\text{field}}$ values be 0.83, 0.92 and 0.99 for R_D values of 33.6, 50.4 and 67.2, respectively. For sand with a relative density of 74.9%, the associated values are 0.75, 0.88 and 0.98. The values suggested by Mayne and Kulhawy [12] are very close to the values predicted from the numerical analyses in this study.

Table 3 also shows that Jamiolkowski et al. [10] proposed the largest value for the $q_{c,cc}/q_{c,\text{field}}$ ratio and Salgado et al. [4] suggested the smallest value. The correction factors predicted numerically in this study for $R_D = 33.6$ are in-between the values suggested empirically by Mayne and Kulhawy [12] and Jamiolkowski et al. [10] and, for higher R_D values, are close to the Mayne and Kulhawy [12] equation.

The empirical relations suggested by Jamiolkowski et al. [10] and Mayne and Kulhawy [12] are only functions of sand relative density and are not influenced by the stress state. Salgado et al. [4] correctly recognized this deficiency in these empirical relations. As Salgado et al. [4] argue, in addition to the sand relative density, the choice of a suitable diameter ratio, at which size effect is no longer important, should also be based on the stress state, as discussed below.

Figures 7a, b and c present a graphical comparison of calibration chamber size effects between the empirical equation of Mayne and Kullhawy [12] (Equation 2) and the numerical analysis carried out in this study. Three categories of sand are considered to be very loose, medium dense and very dense. The abscissa in these figures is the calibration chamber to cone diameter ratio (R_D), and the ordinate is the ratio of $q_{c,cc}/q_{c,\text{field}}$. The very loose sand is characterized by a low value of relative density ($Dr = 30\%$) and a high value of confinement stress ($\sigma'_v = 700$ kPa and $\sigma'_h = 350$ kPa), the very dense sand is characterized by a high value of relative density ($Dr = 90\%$) and a low value of confinement stress ($\sigma'_v = 70$ kPa and $\sigma'_h = 35$ kPa) and the medium dense sand is characterized by values between these extreme case scenarios ($Dr = 60\%$, $\sigma'_v = 240$ kPa and $\sigma'_h = 120$ kPa).

Figure 7a shows that the numerically predicted values of $q_{c,cc}/q_{c,\text{field}}$, as a function of chamber-to-

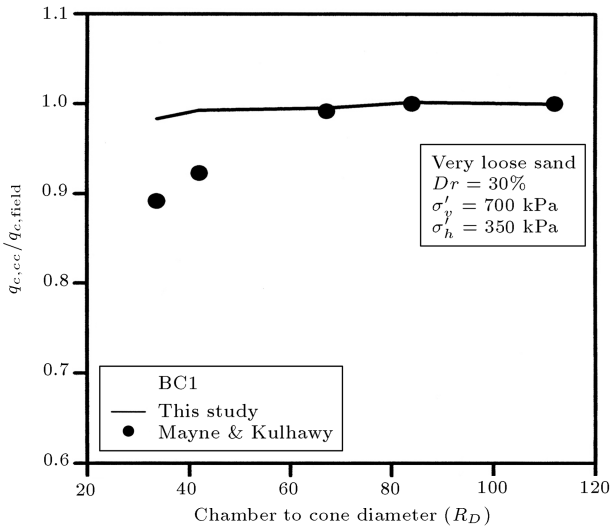

Figure 7a. Comparison of the ratio of $q_{c,cc}/q_{c,\text{field}}$ for very loose sand predicted in numerical analysis in this study and Mayne and Kulhawy's empirical relation [12] (BC1, $Dr = 30\%$, $\sigma'_v = 700$ kPa and $K_0 = 0.5$).

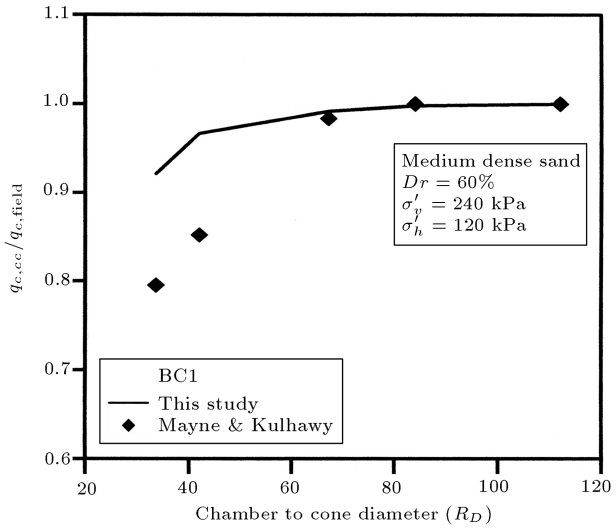

Figure 7b. Comparison between the ratio of $q_{c,cc}/q_{c,\text{field}}$ for medium dense sand predicted in numerical analysis in this study and Mayne and Kulhawy's empirical relation [12] (BC1, $Dr = 60\%$, $\sigma'_v = 240$ kPa and $K_0 = 0.5$).

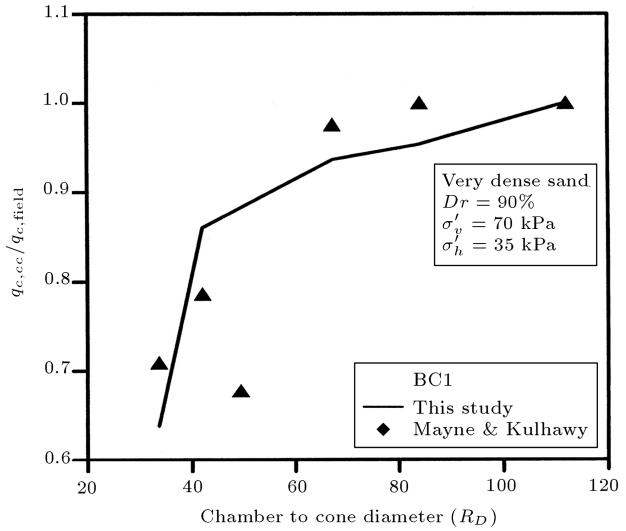

Figure 7c. Comparison between the ratio of $q_{c,cc}/q_{c,\text{field}}$ for very dense sand predicted in numerical analysis in this study and Mayne and Kulhawy's empirical relation [12] (BC1, $Dr = 90\%$, $\sigma'_v = 70$ kPa and $K_0 = 0.5$).

cone diameter ratio for very loose sand (shown by the line), are higher than those obtained from Mayne and Kulhawy [12], which are shown as points. For a chamber-to-cone diameter ratio of 33.6, the predicted value of $q_{c,cc}/q_{c,\text{field}}$ in this study is close to one, but according to Equation 2, is close to 0.9. The predictions in this study and those obtained by Mayne and Kulhawy [12] converge at an R_D value of about 70.

Figure 7b, for medium dense sand, shows a similar trend to the loose sand in Figure 7a. Here, again, it is seen that the numerical predictions produce higher values of $q_{c,cc}/q_{c,\text{field}}$ for low values of R_D and similar values at high values of R_D.

Figure 7c presents the comparison for very dense sand, where the predicted values of $q_{c,cc}/q_{c,\text{field}}$ from this study are reasonably similar to the values using the empirical approach by Mayne and Kulhawy [12].

DISCUSSION

In the following, several aspects of analysis results and applications are discussed.

Effect of Stress State

Figure 8 shows the results of a series of analyses, in which the confining stress, $[= (\sigma'_v + 2\sigma'_h)/3]$, is varied. The type of boundary condition for these series of analyses is BC1 and the sand relative density is 60%, with K_0 equal to 0.5. Figure 8 shows that, as the confining stress increases, the numerically predicted ratio of $q_{c,cc}/q_{c,\text{field}}$ increases and tends toward a value of 1.0. This means that, with the increase in confining stress, the sand becomes less dilatant and behaves more like loose sand with a small zone of influence, and the measured tip resistance is less influenced by the calibration chamber size and boundary conditions. This observation is supported by a basic soil mechanics theory and has been confirmed in the field [24], as well as in similar numerical studies [17].

Figure 8 also shows that, according to Mayne and Kulhawy [12], for sand with a given relative density, the magnitude of $q_{c,cc}/q_{c,\text{field}}$ is a constant value, irrespective of the confinement stress (or sand stress state). This is also true for Jamiolkowski et

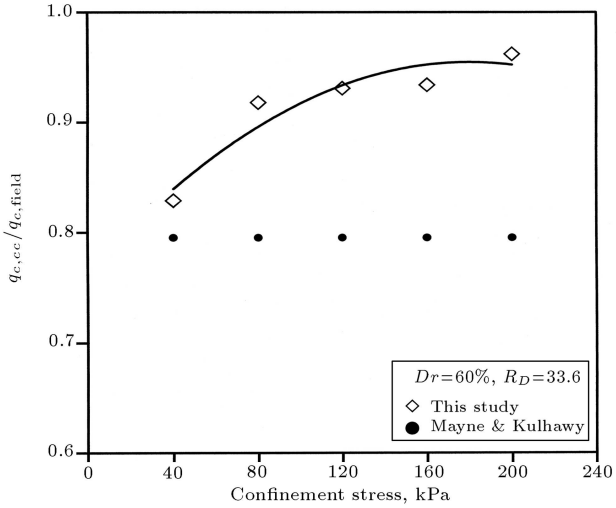

Figure 8. Comparison between the ratio of $q_{c,cc}/q_{c,\text{field}}$ as a function of sand confinement stress $[= (\sigma'_v + 2\sigma'_h)/3]$ predicted in numerical analysis in this study and Mayne and Kulhawy's empirical relation [12] (BC1, $Dr = 60\%$, $R_D = 33.6$ and $K_0 = 0.5$).

al. [10]. The independency of $q_{c,cc}/q_{c,\text{field}}$ to stress state is considered a significant shortcoming of the Jamiolkowski et al. [10] and Mayne and Kulhawy [12] empirical relationships. Therefore, these relations can only be applied to the range of stress states from which they were initially derived.

Practical Measures to Reduce Chamber Size Effects

This study has shown that the calibration chamber size effect is reduced if the chamber-to-cone diameter ratio (R_D) is large. For very dense dilatant sand, an R_D value of 100 or more is required to measure the correct cone tip resistance values in a chamber. However, for most practical purposes, an R_D value of 80 seems to be sufficient for dense sand. This can be seen in Figure 3, where it is shown that, for an R_D value of about 80, the boundary conditions do not affect the tip resistance values significantly. This is also in agreement with Mayne and Kullhawy [12] who, based on experimental observations, suggested a value of 70 for R_D. To satisfy this requirement, either the diameter of the chamber should be enlarged, or the diameter of the cone should be decreased. If the cone has a diameter of 35.7 mm (10 cm^2 cone), the diameter of the chamber should be at least 2.8 m, in order to avoid chamber size effects in dense sand. However, a large calibration chamber of this size is generally not practical or cost effective for calibration chamber testing. It, therefore, appears that decreasing the diameter of the cone could be a better solution. If the diameter of the cone is 20 mm (3.14 cm^2 cone) instead of the standard size of 35.7 mm, the calibration chamber diameter could be 1.6 m., which is close to the conventional calibration chamber size currently available. Ultimately, the cone cannot be reduced to a very small size, due to issues related to cone bending and grain-to-cone diameter effects.

Another approach is to test dense sands under very high stresses to reduce the dilation of the sand and, hence, reduce the zone of influence during cone penetration. However, this often exceeds the range of interest for field stress levels.

What Type of BC in the Chamber Simulates Field Penetration More Closely?

In the previous sections it was shown that, for a given sand with a given relative density and stress state under essentially normally consolidated conditions (i.e. $Ko = 0.5$), the numerically predicted values of tip resistance under BC3 type boundary conditions are slightly larger for smaller values of R_D ratios. This means that the tip resistance values measured in a perfectly rigid wall calibration chamber with BC3 type boundary conditions may be somewhat larger than those which can be measured in the field. However, this may not be the case for flexible wall experimental calibration chambers, where a condition of zero lateral displacement may not be truly achieved. In other words, the boundary condition of zero lateral displacement may not be fully achieved with conventional calibration chambers and, therefore, the q_c values measured in the currently available calibration chambers are not necessarily higher than those which can be measured in the field. The reason for this is that the calibration chambers generally have flexible walls and, as Salgado et al. [13] argued, it is not always possible to experimentally maintain a perfectly rigid circumferential boundary at the calibration chamber walls. This imparts some degree of flexibility to the radial walls, meaning that the BC3 measurements in the chamber may not necessarily be higher for smaller values of R_D ratios. The practical consequence of this flexible vertical boundary is that these types of calibration chamber may, ironically, better simulate field conditions. This statement is supported by the experimental observations of Parkin [25], as shown in Figure 6. It can, therefore, be concluded that field conditions may be simulated reasonably well with this type of flexible wall calibration chamber during test procedures under BC3 type boundary conditions, provided the sand is normally consolidated (Figure 6).

NC SAND VS OC SAND

All analyses carried out in this study are for normally consolidated sand. Generally, the values of K_0 for a normally consolidated sand ranges from 0.4 to 0.5. As described previously, the value of K_0 for all analyses is assumed to be a constant value equal to 0.5, which is in the range of K_0 values expected for normally consolidated sand. Although an important consideration, the emphasis in this study is not on the effects of K_0 on the calibration chamber size and boundary conditions. This is also true for previous numerical or empirical relations, with which the results of the present study were compared. It is, therefore, noted that the conclusions drawn from this study should only be limited to normally consolidated sand. Further research is needed for over-consolidated sand with higher values of K_0 and higher values of horizontal effective stresses.

CONCLUSIONS

A numerical approach was carried out to study the effects of chamber size and boundary conditions on cone tip resistance values in NC sand. Analyses were presented for normally consolidated dense, medium

dense and loose sand. The numerical results were compared with other empirical and numerical procedures available in the literature.

The analysis presented in this study, together with experimental measurements, indicates that the ratio of chamber-to-cone diameter (R_D) is a primary factor in influencing cone tip resistance measurements in the chamber, especially for dense sand samples. The higher this ratio is, the less significant the size and boundary effects are.

For normally consolidated dense sand under BC1 and BC4 boundary conditions, numerical results show that the tip resistance increases as the ratio of chamber-to-cone diameter increases. For BC2 boundary conditions, the predicted tip resistance decreases as the chamber-to-cone diameter increases and, for BC3 boundary conditions, the predicted tip resistance is somewhat larger for smaller values of R_D and shows a decreasing trend as the R_D ratio increases.

The difference in predicted tip resistance values for boundary conditions BC1 (or BC4) and BC2 obtained in the analyses for medium dense sand, is appreciably less than that obtained for very dense sand. For loose sand, this difference is even smaller. These results imply that the zone of influence around a penetrating cone in sand is small if the sand is very loose, but large when the sand is very dense. The results also imply that, as the confining stress increases, dense sand behaves more like loose sand.

The numerical results in this study show that, in very dense and dilatant sand (i.e. low stress level), a chamber-to-cone diameter ratio of more than 100 is required in order to observe the lack of effect of chamber boundaries on tip resistance values. However, for practical purposes, an R_D value of 80 seems to be satisfactory for dense sand. For medium dense sand, smaller values of chamber-to-cone diameter ratios appear sufficient, so that cone tip resistance measurements are not affected by the boundaries.

The results of this study are compared with the numerical results of Salgado et al. [4] and the empirical relations suggested by Jamiolkowski et al. [10] and Mayne and Kulhawy [12]. It is seen that the Salgado et al. [4] procedure predicts ratios that are significantly smaller than the values predicted in this study and Jamiolkowski et al. [10] proposed the largest value for the $q_{c,cc}/q_{c,\text{field}}$ ratio. The correction factors predicted numerically in this study for $R_D = 33.6$ are in-between the values suggested empirically by Mayne and Kulhawy [12] and Jamiolkowski et al. [10] and, for higher R_D values, they are close to the Mayne and Kulhawy [12] equation. The empirical relationships suggested by Mayne and Kulhawy [12] and Jamiolkowski et al. [10] are not influenced by the stress state of the sand. This is considered to be a shortcoming in these empirical relations.

NOMENCLATURE

K	bulk modulus
BC1	boundary condition type 1 in calibration chamber, σ_h = constant, σ_v = constant
BC2	boundary condition type 2 in calibration chamber, $\varepsilon_h = 0$, $\varepsilon_v = 0$
BC3	boundary condition type 3 in calibration chamber, $\varepsilon_h = 0$, σ_v = constant
BC4	boundary condition type 4 in calibration chamber, $\varepsilon_v = 0$, σ_h = constant
CPT	acronym for "Cone Penetration Test"
Dr	relative density of the sand in the chamber before penetration and after consolidation
FLAC	a computer program, acronym for "Fast Lagrangian Analysis of Continua"
E	Young's elastic modulus
G	shear modulus of soil
K_B	bulk stiffness number
K_G	shear stiffness number
K_0	coefficient of earth pressure at rest, or coefficient of lateral stress before penetration
n	stress exponent
OCR	over-consolidation ratio
P_A	atmospheric pressure
q_c	cone tip resistance
$q_{c,cc}$	cone tip resistance measured in calibration chamber
$q_{c,\text{field}}$	cone tip resistance expected to be measured in the field
R_D	ratio of chamber diameter to cone diameter
α	angle which describes the curvature of the failure envelope
ϕ_{cv}	constant volume friction angle
ϕ'_f	effective friction angle at failure
ϕ'_0	secant angle of friction at $\sigma'_{ff} = 2.72\ P_A$
ψ	dilation angle
σ'_{ff}	effective normal stress on the failure surface at failure
σ'_h	effective horizontal stress
σ'_m	mean effective stress
σ'_v	effective vertical stress
τ_{ff}	shear stress on the failure surface at failure
ν	Poisson's ratio

REFERENCES

1. Holden, J.C. "History of the first six CRB calibration chambers", *Proceeding of the First International Symposium on Calibration Chamber Testing*, Potsdam, New York, pp 1-11 (1991).
2. Bellotti, R., Bizzi, G. and Ghionna, V. "Design, construction, and use of a calibration chamber", *Proceedings of the 2nd European Symposium on Penetration Testing (ESOPT II)*, Amsterdam, **2**, pp 439-446 (1982).
3. Bellotti, R., Crippa, V., Pedroni, S. and Ghionna, V.N. "Saturation of sand specimen for calibration chamber tests", *Proceedings of the First International Symposium on Penetration Testing (ISOPT)*, **2**, pp 661-671 (1988).
4. Salgado, R., Mitchell, J.K. and Jamiolkowski, M. "Calibration chamber size effects on penetration resistance in sand", *Journal of Geotechnical and Geoenvironmental Engineering, ASCE*, **124**(9), pp 878-888 (1998).
5. Ghionna, V. and Jamiolkowski, M. "A critical apraisal of calibration chamber testing of sands", *Proceedings of the First International Symposium on Calibration Chamber Testing*, Potsdam, New York, pp 13-39 (1991).
6. Been, K., Crooks, J.H.A. and Rothenburg, L. "A critical appraisal of CPT calibration chamber tests", *Proceeding of the First International Symposium on Penetration Testing (ISOPT)*, **2**, pp 651-660 (1988).
7. Parkin, A.K. and Lunne, T. "Boundary effects in the laboratory calibration of a cone penetrometer in sand", *Proceedings of the 2nd European Symposium on Penetration Testing (ESOPT II)*, Amsterdam, **2**, pp 761-768 (1982).
8. Lunne, T. and Christophersen, H.P. "Interpretation of cone penetration data for offshore sands", *Proceedings of 15th Annual Offshore Technology Conference*, Houston, Texas, pp 181-192 (1983).
9. Hsu, H.H. and Huang, A.B. "Development of an axisymmetric field simulator for cone penetration tests in sand", *Geotechnical Testing Journal*, **21**(4), pp 348-355 (1998).
10. Jamiolkowski, M., Ladd, C.C., Germaine, J.T. and Lancellotta, R. "New developments in field and laboratory testing of soils", *Proceedings of 11th International Conference on Soil Mechanics and Foundation Engineering*, San Francisco, pp 57-154 (1985).
11. Schnaid, F. and Houlsby, G.T. "An assessment of chamber size effects in the calibration of in-situ tests in sand", *Geotechnique*, **41**(3), pp 437-445 (1991).
12. Mayne, P.W. and Kulhawy, F.H. "Calibration chamber data base and boundary effects correction for CPT data", *Proceedings of the First International Symposium on Calibration Chamber Testing*, Potsdam, New York, pp 257-264 (1991).
13. Salgado, R., Mitchell, J.K. and Jamiolkowski, M. "Cavity expansion and penetration resistance in sand", *Journal of Geotechnical and Geoenvironmental Engineering, ASCE*, **123**(4), pp 344-354 (1997).
14. Wesley, L.D. "Interpretation of calibration chamber tests involving cone penetrometers in sands", *Geotechnique*, **52**(4), pp 289-293 (2002).
15. Ahmadi, M.M. "Analysis of cone tip resistance in sand", PhD Thesis, University of British Columbia, Vancouver, Canada (2000).
16. Ahmadi, M.M., Byrne, P.M. and Campanella, R.G. "Cone tip resistance in sand: Modeling, verification, and applications", *Canadian Geotechnical Journal*, **42**, pp 977-993 (2005).
17. Ahmadi, M.M. and Robertson, P.K. "Thin layer effects on the CPT q_c measurement", *Canadian Geotechnical Journal*, **42**, pp 1302-1317 (2005).
18. FLAC User Manual, version 4.0, Itasca Consulting Group Inc., USA (2000).
19. Baligh, M.M., *Theory of Deep Site Static Cone Penetration Resistance*, Publication No. R75-56, Department of Civil Engineering, Massachusetts Institute of Technology (1975).
20. Byrne, P.M., Cheung, H. and Yan, L. "Soil parameters for deformation analysis of sand masses", *Canadian Geotechnical Journal*, **24**, pp 366-376 (1987).
21. Baldi, G., Bellotti, R., Ghionna, V., Jamiolkowski, M. and Pasqualini, E. "Interpretations of CPT's and CPTU's, 2nd Part: Drained penetration of sands", *4th International Conference on Field Instrumentation and In-situ Measurements*, Singapore, pp 143-156 (1986).
22. Lo Presti, D.C.F., Pedroni, S. and Crippa, V. "Maximum dry density of cohesionless soils by pluviation and by ASTM D 4253-83: A comparative study", *Geotechnical Testing Journal*, **15**(2), pp 180-189 (1992).
23. van den Berg, P. "Analysis of soil penetration", PhD Thesis, Delft University of Technology, Netherlands (1994).
24. Lunne, T., Robertson, P.K. and Powell, J.M. "Cone penetration testing in geotechnical practice", *Blackie Academic & Professional* (1997).
25. Parkin, A.K. "The calibration of cone penetrometers", *Proceedings of the First International Symposium on Penetration Testing (ISOPT)*, **1**, pp 221-243.